

Ferromagnetic spin-polaron on complex lattices

Mona Berciu and George A. Sawatzky

Department of Physics and Astronomy, University of British Columbia, Vancouver, BC, Canada, V6T 1Z1

(Dated: November 23, 2018)

We present a simpler derivation of the exact solution of a spin-polaron in a ferromagnet and generalize it to complex lattices and/or longer range exchange interactions. As a specific example, we analyze a two-dimensional MnO_2 -like lattice (as in the ferromagnetic layers in LaMnO_3) and discuss the properties of the resulting spin-polaron in various regimes. At strong couplings the solution is reminiscent of the Zhang-Rice singlet, however the electronic wavefunction involved in the singlet is dependent on the momentum of the singlet, and multiple bands may appear.

PACS numbers: 71.10.Fd, 71.27.+a, 75.50.Dd

I. INTRODUCTION

The motion of a charged particle in a magnetically ordered background is one of the central basic problems encountered in doped, magnetically ordered insulators. Well known examples are hole or electron doped ferromagnetic insulators such as EuO ,¹ hole doped parent compounds of the colossal magneto-resistance materials,² hole and electron doped parent compounds of high-temperature superconductors,^{3,4} etc.

The exact solution of the problem in a two-dimensional (2D) antiferromagnetic lattice as represented by the cuprates still eludes us. Diagrammatic Quantum Monte Carlo calculations on an assumed Neel-ordered lattice and in a single band tJ -like model provide an exact numerical solution to this approximated system.⁵ In the real system, however, the hole propagates in an O $2p$ band while the spins are a result of a half-filled Cu $d_{x^2-y^2}$ band with a large Hubbard U .

The other examples like EuO or LaMnO_3 are either ferromagnetic or, as in the case of LaMnO_3 , have ferromagnetic 2D layers. As we show here, for these systems there is an exact solution available for a hole or electron propagating in either the same, or a different band from that of the spin background, and for any sign and magnitude of the coupling. Exact solutions of this kind provide important information on the existence range of bound spin-polaron states as envisioned for example for Zhang-Rice (ZR) singlets,⁶ in which the hole propagates in an O sublattice and the local spins are on a transition metal (TM) sublattice. It is important to note that aside from cuprates, there is evidence that doped holes in manganites LaMnO_3 and cobaltates Na_xCoO_2 also propagate on the O sublattice but are strongly coupled to the TM.

Indeed, it has been known for a long time^{7,8,9,10,11,12} that an exact solution can be found for the Green's function of a particle (electron or hole) moving in a lattice of ferromagnetically (FM) ordered spins, at zero temperature. If the spin of the particle is parallel to the FM order, the solution is trivial: its energy is simply shifted by its exchange coupling to the FM spins. However, if the particle spin is antiparallel to the FM order, it can scatter and spin-flip by creating a magnon. Depending on the values of the various parameters and the total energy, this can

result in a finite lifetime (incoherent scattering leading to a broad spectral weight) or in an infinitely-lived quasiparticle – the spin-polaron – comprising the bound-state of the particle and the magnon. In the later case, the dispersion of the spin-polaron can be significantly renormalized compared to that of the free particle.

Similar physics is found in a seemingly more complex Kondo-Anderson model that also admits an exact solution.¹³ This is not surprising, because the restriction placed there on the allowed occupation numbers of the d orbitals essentially maps it back to an electron interacting with FM-ordered spins. Effort has also been focused on trying to extend this type of solution to finite-temperature (*i.e.* presence of multiple magnons), to finite particle concentrations, etc. While, to our knowledge, no other exact solutions have been found, such work has resulted in various approximations for the self-energy.¹⁴

One common aspect of all these exact solutions are the assumptions (1) that the particle moves on the same lattice that hosts the FM spins (usually a simple cubic-like lattice in d dimensions, although generalizations to other cases are trivial), and (2) that the particle-spin exchange is local, *i.e.* purely on-site.

In this article we show that the $T = 0$ exact solution can be generalized to systems where these restrictions are lifted. In other words, to cases where the particle moves on the same lattice that hosts the FM spins but the exchange is longer range, as well as to cases where the particle moves on a different sublattice than the one hosting the FM spins so that the exchange is necessarily not on-site. We focus on a specific problem of the later type, and briefly comment on other possible generalizations later on. While our formalism is similar in spirit to that used in Refs. 7,8,9,10,11,12, it is in practice much simpler to use and more transparent. This is essential to allow us to find these generalized exact solutions.

Such calculations are necessary in order to understand quantitatively direct/inverse angle-resolved photoemission spectroscopy (ARPES) (when the particle is a hole/electron), in insulators which order ferromagnetically, for instance oxides like EuO , CuCr_2S_4 , CuCr_2Se_4 , MgFe_2O_4 , etc. They may also be relevant to some extent for itinerant ferromagnets, given that spin-polarized electron loss spectroscopy on thin Co films¹⁵ reveals good fits

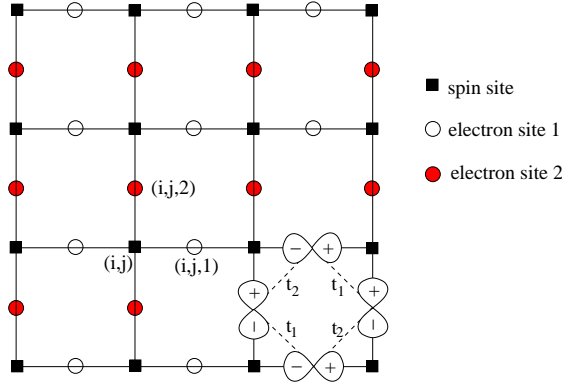


FIG. 1: Sketch of the lattice and the indexes of sites in the unit cell. The bottom-right cell shows the signs of the p orbital lobes, which define the signs of the hopping integrals t_1, t_2 .

of the measured spin-wave spectrum to effective Heisenberg models, however more work needs to be done to understand how to properly extend it in this direction.

Our results suggest possible spintronic uses for these materials, in terms of transport of spin-polarized currents, since we prove that charge carriers with spin-polarization antiparallel to that of the FM background can propagate *coherently*, in other words scattering on magnons is not necessarily leading to a finite lifetime. Equally importantly, the results also give some useful insights on ways to improve our understanding of the propagation of electrons or holes in antiferromagnetic backgrounds. These issues are discussed in more detail below.

The paper is organized as follows: in section II we introduce the specific model to be solved. In section III we give its exact solution, and comment on various possible generalizations. In section IV we present and analyze a selection of interesting results. Section V contains our summary and conclusions.

II. MODEL

We study the 2D model of Fig. 1. It consists of two sublattices: the one hosting the FM-ordered spins is a simple square lattice of lattice constant a , whose sites are marked by black squares (the analogs of the Mn sites in a MnO_2 lattice). The charge carrier is moving on the other sublattice, which includes all the sites marked by circles (the analogs of O sites in a MnO_2 lattice). The spin of the charge carrier is coupled through exchange to the spins on its two nearest neighbor sites.

Such a model would describe for example a MnO_2 layer of the parent compound LaMnO_3 if it was modeled as a charge-transfer insulator.¹⁶ The Mn ions are in the $3d^4$ ($S = 2$) configuration, and have ferromagnetic order in each layer. In a charge-transfer insulator, doping would introduce a hole in the O $2p$ orbitals instead of emptying an e_g Mn $3d$ orbital. The spin of the hole would be AFM coupled to the neighboring Mn spins, with a $J_0 \sim$

$|t_{p-d}|^2/\Delta E$, where t_{p-d} would measure the hybridization of the orbitals, and ΔE would be the overall energetic cost to move the hole to a Mn site.

This model is also reminiscent of the CuO_2 layers of cuprate parent compounds, which are charge transfer materials with holes going into O $2p$ orbitals. In this case, $S = 1/2$ for the $3d^9$ configuration of the Cu in the insulator, however of course these spins order antiferromagnetically, not FM as assumed to be the case here.

In any event, our primary motivation here is to exemplify the general solution for these types of problems, and we chose this model Hamiltonian because it is complex enough to demonstrate the full power of our solution, yet simple enough not to make the notations too cumbersome. It also unveils some very interesting physics. The solution can be directly generalized to a much wider class of similar problems, as discussed below, and can therefore be used to describe realistic systems.

We assume a total of N unit cells, with periodic boundary conditions. In all our results we let $N \rightarrow \infty$. Each unit cell is indexed by a pair of integers (i, j) and contains three sites: a spin site located at $\vec{R}_{ij} = ia\hat{x} + ja\hat{y}$ and 2 inequivalent electron sites, denoted 1 (for the site on the x -rung, location $\vec{R}_{ij,1} = \vec{R}_{ij} + \frac{a}{2}\hat{x}$) and 2 (site on the y -rung, location $\vec{R}_{ij,2} = \vec{R}_{ij} + \frac{a}{2}\hat{y}$).

The hopping between the various electron sites is also indicated in Fig. 1. For simplicity we limit ourselves to nearest-neighbor hopping – generalizations are straightforward. If the orbitals occupied by the charge carrier are p -orbitals (as drawn), then one must take $t_1 = -t_2 = t$, whereas if they are s -type orbitals (not shown), one should choose $t_1 = t_2 = t$. In any event, we will use general t_1 and t_2 values for the derivation. The difference between a hole vs. an electron charge carrier is the sign of t : $t > 0$ for electrons, and $t < 0$ for holes. At first sight one would think that the sign of t is irrelevant, since the model is particle-hole symmetric. In fact, while the energetics is the same, the sign is important for the wavefunctions and therefore has interesting consequences.

In the following, we assume that the charge carrier is an electron, and we will comment on the differences for holes where appropriate.

We introduce the Fourier-transformed operators

$$c_{\vec{k},\lambda,\sigma}^\dagger = \frac{1}{\sqrt{N}} \sum_{i,j} e^{i\vec{k}\vec{R}_{ij,\lambda}} c_{ij,\lambda,\sigma}^\dagger \quad (1)$$

where $c_{ij,\lambda,\sigma}^\dagger$ creates an electron with spin σ at site $\lambda = 1, 2$ of the (i, j) unit cell. In terms of these, the nearest-neighbor hopping of the electron is written simply as:

$$\hat{T} = \sum_{\vec{k},\sigma} \epsilon_{\vec{k}} \left(c_{\vec{k},1,\sigma}^\dagger c_{\vec{k},2,\sigma} + h.c. \right) \quad (2)$$

where the sum is over the allowed values of \vec{k} in the first Brillouin zone (BZ) $(-\frac{\pi}{a}, \frac{\pi}{a}] \times (-\frac{\pi}{a}, \frac{\pi}{a}]$, and

$$\epsilon_{\vec{k}} = -2t_1 \cos \frac{(k_x - k_y)a}{2} - 2t_2 \cos \frac{(k_x + k_y)a}{2}. \quad (3)$$

The hopping Hamiltonian is diagonalized trivially by using the new operators

$$c_{\vec{k},\pm,\sigma} = \frac{1}{\sqrt{2}} \left(c_{\vec{k},1,\sigma} \pm c_{\vec{k},2,\sigma} \right), \quad (4)$$

in terms of which the hopping Hamiltonian is:

$$\hat{T} = \sum_{\vec{k},\sigma} \epsilon_{\vec{k}} \left(c_{\vec{k},+,\sigma}^\dagger c_{\vec{k},+,\sigma} - c_{\vec{k},-,\sigma}^\dagger c_{\vec{k},-,\sigma} \right). \quad (5)$$

As expected for this two-site unit cell, there are two bands for the free electron (they happen to touch, there is no gap between them). If $t_1 = t_2$ (s-orbitals), the ground-state is at the Γ -point $k_x = k_y = 0$. If $t_1 = -t_2$ (p-orbitals), the ground-state is moved to $k_x = k_y = \pi/a$ or equivalent points at the corners of the Brillouin zone. In fact, the whole dispersion is just translated by $\frac{\pi}{a}(1,1)$ inside the Brillouin zone, hence the resulting physics is exactly the same in both cases. Differences between s - and p -orbitals (besides this overall shift) are only apparent if there is longer range hopping. Since we do not consider longer-range hopping here, in the following we will report results for the s -orbital case $t_1 = t_2$.

To the hopping term, we add the FM Heisenberg exchange between the spins of magnitude S :

$$\mathcal{H}_{\text{spins}} = -J \sum_{i,j} \left[\vec{S}_{i,j} \vec{S}_{i,j+1} + \vec{S}_{i,j} \vec{S}_{i+1,j} - 2S^2 \right] \quad (6)$$

where the sum runs over all units cells (we limit ourselves to nearest-neighbor exchange since generalizations to longer-range exchange are trivial, so long as there is no frustration) and the electron-spin exchange:

$$\mathcal{H}_{\text{exc}} = J_0 \sum_{i,j} \left[\vec{s}_{ij,1} \cdot \left(\vec{S}_{ij} + \vec{S}_{i+1,j} \right) + \vec{s}_{ij,2} \cdot \left(\vec{S}_{ij} + \vec{S}_{i,j+1} \right) \right] \quad (7)$$

where $\vec{s}_{ij,\lambda} = \sum_{\alpha,\beta} c_{ij,\lambda,\alpha}^\dagger \frac{\vec{\sigma}_{\alpha\beta}}{2} c_{ij,\lambda,\beta}$ is the spin of the electron at site $\lambda = 1, 2$ of the (ij) unit cell.

The total Hamiltonian is the sum of the three terms of Eqs. (5), (6) and (7). For later convenience, we divide it in two parts:

$$\mathcal{H} = \mathcal{H}_0 + V \quad (8)$$

where

$$\mathcal{H}_0 = \hat{T} - J \sum_{i,j} \left[S_{i,j}^z S_{i,j+1}^z + S_{i,j}^z S_{i+1,j}^z - 2S^2 \right] \quad (9)$$

includes the hopping and the diagonal (zz) part of the FM Heisenberg interaction between the spins. V includes the remaining terms, *i.e.* the xy part of the FM exchange between spins, and the coupling of the electron spin to the spins located on its two neighboring sites.

III. THE GREEN'S FUNCTION OF THE SPIN-POLARON

We consider the case where a single electron is in the system and $T = 0$. Let $|\text{FM}\rangle = | +S, +S, \dots, +S \rangle$ be the ground-state of the spins, in the absence of the electron. If the electron has spin-up the problem is trivially solved, since the xy parts of all exchanges have zero action in this subspace (no spins can be flipped). We therefore only treat explicitly the case of a spin-down electron.

We define

$$\Psi_{\vec{k},\sigma} = \begin{pmatrix} c_{\vec{k},1,\sigma} \\ c_{\vec{k},2,\sigma} \end{pmatrix} \quad (10)$$

and introduce the 2×2 Green's function matrix:

$$\bar{G}(\vec{k}, \omega) = \langle \text{FM} | \Psi_{\vec{k},\downarrow} \hat{G}(\omega) \Psi_{\vec{k},\downarrow}^\dagger | \text{FM} \rangle, \quad (11)$$

where the resolvent is $\hat{G}(\omega) = 1/(\omega - \mathcal{H} + i\eta)$, with $\eta > 0$ infinitesimally small, and we hereafter set $\hbar = 1$. This shorthand notation means, for example, that the (1,2) element of this matrix is:

$$G_{1,2}(\vec{k}, \omega) = \langle \text{FM} | c_{\vec{k},1,\downarrow} \hat{G}(\omega) c_{\vec{k},2,\downarrow}^\dagger | \text{FM} \rangle$$

etc., so that all four possible combinations are considered at once. Using a Lehman representation,¹⁷ it is clear that

$$G_{\lambda,\lambda'}(\vec{k}, \omega) = \sum_u \frac{\langle \text{FM} | c_{\vec{k},\lambda,\downarrow} | u \rangle \langle u | c_{\vec{k},\lambda',\downarrow}^\dagger | \text{FM} \rangle}{\omega - E_u + i\eta}$$

where $\mathcal{H}|u\rangle = E_u|u\rangle$ are the single-electron eigenstates in the sector of total z -axis spin $NS - \frac{1}{2}$. In other words, the poles of these quantities give all the eigenenergies and the residues measure overlaps between the true eigenfunctions and the appropriate free-electron state $c_{\vec{k},\lambda,\downarrow}^\dagger | \text{FM} \rangle$, $\lambda = 1, 2$.

Our goal is to calculate exactly this Green's function matrix. We do this by using repeatedly Dyson's identity $\hat{G}(\omega) = \hat{G}_0(\omega) + \hat{G}(\omega) V \hat{G}_0(\omega)$, where $\hat{G}_0(\omega) = 1/(\omega - \mathcal{H}_0 + i\eta)$ and \mathcal{H}_0 is defined in Eq. (9).

Rotating to the diagonal basis $c_{\vec{k},\pm,\downarrow}$ [see Eq. (4)] and back, it is straightforward to show that:

$$\hat{G}_0(\omega) \Psi_{\vec{k},\downarrow}^\dagger | \text{FM} \rangle = \Psi_{\vec{k},\downarrow}^\dagger | \text{FM} \rangle \bar{G}_0(\vec{k}, \omega) \quad (12)$$

where we introduce the 2×2 matrix:

$$\bar{G}_0(\vec{k}, \omega) = \begin{pmatrix} G_0^{(+)}(\vec{k}, \omega) & G_0^{(-)}(\vec{k}, \omega) \\ G_0^{(-)}(\vec{k}, \omega) & G_0^{(+)}(\vec{k}, \omega) \end{pmatrix} \quad (13)$$

in terms of the known free-electron propagators:

$$G_0^{(\pm)}(\vec{k}, \omega) = \frac{1}{2} \left[\frac{1}{\omega - \epsilon_{\vec{k}} + i\eta} \pm \frac{1}{\omega + \epsilon_{\vec{k}} + i\eta} \right]. \quad (14)$$

Using Dyson's identity once thus leads to the equation:

$$\bar{G}(\vec{k}, \omega) = \left[1 + \langle \text{FM} | \Psi_{\vec{k},\downarrow} \hat{G}(\omega) V \Psi_{\vec{k},\downarrow}^\dagger | \text{FM} \rangle \right] \bar{G}_0(\vec{k}, \omega).$$

Since the objects appearing here are 2×2 matrices, the order of multiplications in these equations is important.

The action of V on $\Psi_{\vec{k},\downarrow}^\dagger |\text{FM}\rangle$ is easily estimated. The xy exchange between spins has no contribution, since all spins are up. As a result, one finds contributions only due to the electron-spins exchange, resulting in:

$$\bar{G}(\vec{k}, \omega) = \bar{G}_0(\vec{k}, \omega) + \left[-J_0 S \bar{G}(\vec{k}, \omega) + \frac{J_0}{N} \sum_{\vec{q}} \bar{F}(\vec{k}, \vec{q}, \omega) \bar{g}(\vec{q}) \right] \bar{G}_0(\vec{k}, \omega) \quad (15)$$

The first term in the square bracket comes from the diagonal zz exchange and corresponds to a simple shift in the total electron energy (see below). The second term comes from the xy exchange, which allows one spin to be lowered by 1, while the electron-spin is flipped to $\sigma = \uparrow$. This leads to a new 2×2 Green's function matrix:

$$\bar{F}(\vec{k}, \vec{q}, \omega) = \sum_{i,j} e^{i\vec{q}\vec{R}_{ij}} \langle \text{FM} | \Psi_{\vec{k},\downarrow}^\dagger \hat{G}(\omega) \Psi_{\vec{k}-\vec{q},\uparrow}^\dagger S_{ij}^- | \text{FM} \rangle.$$

Finally, the diagonal matrix:

$$\bar{g}(\vec{q}) = \begin{pmatrix} \cos \frac{q_x a}{2} & 0 \\ 0 & \cos \frac{q_y a}{2} \end{pmatrix} \quad (16)$$

appears in Eq. (15) because the spin at site (ij) can be flipped by exchange with an electron present at either of the $(ij, 1), (ij, 2), (i-1, j, 1)$ or $(i, j-1, 2)$ sites, which are displaced by $\pm a\hat{x}/2$ or $\pm a\hat{y}/2$ from it [see Eq. (1) for the definition of the phases in the Fourier transforms].

Given the structure of the \bar{G}_0 matrix, it follows that $[\bar{G}_0(\vec{k}, \omega)]^{-1} + J_0 S = [\bar{G}_0(\vec{k}, \omega + J_0 S)]^{-1}$, so we can further simplify Eq. (15) to:

$$\bar{G}(\vec{k}, \omega) = \left[1 + \frac{J_0}{N} \sum_{\vec{q}} \bar{F}(\vec{k}, \vec{q}, \omega) \bar{g}(\vec{q}) \right] \bar{G}_0(\vec{k}, \omega + J_0 S). \quad (17)$$

This shows that an equation for \bar{F} is needed to solve the problem. Using Dyson's identity again, we find, after very similar kinds of manipulations, that its equation of motion is:

$$\bar{F}(\vec{k}, \vec{q}, \omega) = 2J_0 S \bar{G}(\vec{k}, \omega) \bar{g}(\vec{q}) \bar{G}_0(\vec{k} - \vec{q}, \omega - \Omega_{\vec{q}} - J_0 S) - \frac{J_0}{N} \sum_{\vec{Q}} \bar{F}(\vec{k}, \vec{Q}, \omega) \bar{g}(\vec{Q} - \vec{q}) \bar{G}_0(\vec{k} - \vec{q}, \omega - \Omega_{\vec{q}} - J_0 S) \quad (18)$$

where

$$\Omega_{\vec{q}} = 4JS \left(\sin^2 \frac{q_x a}{2} + \sin^2 \frac{q_y a}{2} \right) \quad (19)$$

is the one-magnon spectrum for this FM spin lattice.

Eqs. (17) and (18) can now be solved to find $\bar{G}(\vec{k}, \omega)$ and $\bar{F}(\vec{k}, \omega)$. Note that usually there is an infinite sequence of equations-of-motion connected to one another. In this problem, the series is truncated to just 2 equations because of symmetries: since $\hat{S}_{z,\text{tot}}$ (which includes all spins and the electron) commutes with the Hamiltonian, the evolution is always within the Hilbert sector with z -axis spin $NS - 1/2$. This only includes the states with all spins up and the electron with spin-down; or the electron has spin-up, and then one spin is lowered by one (one magnon is created in the system). This also explains why generalizations to finite T (multiple magnons) or finite electron concentrations are far from trivial: in those cases, more and more equations of motion are generated as the size of the relevant Hilbert subspace increases substantially, and their solution becomes very difficult.

Eqs. (17) and (18) can be solved analytically because of the simple structure of the \bar{g} -matrix, which contains only trigonometric functions. In fact, if we also define:

$$\tilde{g}(\vec{q}) = \begin{pmatrix} \sin \frac{q_x a}{2} & 0 \\ 0 & \sin \frac{q_y a}{2} \end{pmatrix} \quad (20)$$

then we can “factorize”:

$$\bar{g}(\vec{Q} - \vec{q}) = \bar{g}(\vec{Q}) \bar{g}(\vec{q}) + \tilde{g}(\vec{Q}) \tilde{g}(\vec{q}) \quad (21)$$

since $\cos \frac{(Q-q)a}{2} = \cos \frac{Qa}{2} \cos \frac{qa}{2} + \sin \frac{Qa}{2} \sin \frac{qa}{2}$.

We define the auxiliary quantities:

$$\bar{f}(\vec{k}, \omega) = \frac{1}{N} \sum_{\vec{Q}} \bar{F}(\vec{k}, \vec{Q}, \omega) \bar{g}(\vec{Q}), \quad (22)$$

which is the only quantity we need to compute \bar{G} , see Eq. (17), and

$$\tilde{f}(\vec{k}, \omega) = \frac{1}{N} \sum_{\vec{Q}} \bar{F}(\vec{k}, \vec{Q}, \omega) \tilde{g}(\vec{Q}) \quad (23)$$

in terms of which we can rewrite Eq. (18) as:

$$\bar{F}(\vec{k}, \vec{q}, \omega) = J_0 \left[-\bar{f}(\vec{k}, \omega) \bar{g}(\vec{q}) - \tilde{f}(\vec{k}, \omega) \tilde{g}(\vec{q}) + 2S \bar{G}(\vec{k}, \omega) \bar{g}(\vec{q}) \right] \bar{G}_0(\vec{k} - \vec{q}, \omega - \Omega_{\vec{q}} - J_0 S) \quad (24)$$

Substituting this in Eqs. (22) and (23), we obtain two linear (matrix) equations with unknowns \bar{f} and \tilde{f} , and inhomogeneous terms proportional to \bar{G} :

$$\bar{f}(\vec{k}, \omega) = \left[-J_0 \bar{f}(\vec{k}, \omega) + 2J_0 S \bar{G}(\vec{k}, \omega) \right] \bar{g}_{11}(\vec{k}, \omega) - J_0 \tilde{f}(\vec{k}, \omega) \bar{g}_{21}(\vec{k}, \omega)$$

and

$$\tilde{f}(\vec{k}, \omega) = \left[-J_0 \tilde{f}(\vec{k}, \omega) + 2J_0 S \bar{G}(\vec{k}, \omega) \right] \bar{g}_{12}(\vec{k}, \omega) - J_0 \tilde{f}(\vec{k}, \omega) \bar{g}_{22}(\vec{k}, \omega)$$

where we introduced the known 2×2 matrices:

$$\bar{g}_{11}(\vec{k}, \omega) = \frac{1}{N} \sum_{\vec{q}} \bar{g}(\vec{q}) \bar{G}_0(\vec{k} - \vec{q}, \omega - \Omega_{\vec{q}} - J_0 S) \bar{g}(\vec{q}) \quad (25)$$

$$\bar{g}_{12}(\vec{k}, \omega) = \frac{1}{N} \sum_{\vec{q}} \bar{g}(\vec{q}) \bar{G}_0(\vec{k} - \vec{q}, \omega - \Omega_{\vec{q}} - J_0 S) \tilde{g}(\vec{q}) \quad (26)$$

$$\bar{g}_{21}(\vec{k}, \omega) = \frac{1}{N} \sum_{\vec{q}} \tilde{g}(\vec{q}) \bar{G}_0(\vec{k} - \vec{q}, \omega - \Omega_{\vec{q}} - J_0 S) \bar{g}(\vec{q}) \quad (27)$$

$$\bar{g}_{22}(\vec{k}, \omega) = \frac{1}{N} \sum_{\vec{q}} \tilde{g}(\vec{q}) \bar{G}_0(\vec{k} - \vec{q}, \omega - \Omega_{\vec{q}} - J_0 S) \tilde{g}(\vec{q}) \quad (28)$$

In fact, lots of these matrices' elements are related to each other by various symmetries, so fewer than 16 actually need to be calculated. Letting $N \rightarrow \infty$, then each of these corresponds to a two-dimensional integral over the Brillouin zone. One integral can be performed analytically, and the second we integrated numerically, therefore these matrices are easy to calculate.

These coupled equations are easy to solve and the resulting expression of \bar{f} can now be used in Eq. (17) to find the Green's function explicitly. The final result is:

$$\bar{G}(\vec{k}, \omega) = \left[\left(\bar{G}_0(\vec{k}, \omega + J_0 S) \right)^{-1} - 2S J_0 \left(1 - \left(\bar{M}(\vec{k}, \omega) \right)^{-1} \right) \right]^{-1} \quad (29)$$

where we introduced the matrix:

$$\bar{M}(\vec{k}, \omega) = 1 + J_0 \left[\bar{g}_{11}(\vec{k}, \omega) - J_0 \bar{g}_{12}(\vec{k}, \omega) \left(1 + J_0 \bar{g}_{22}(\vec{k}, \omega) \right)^{-1} \bar{g}_{21}(\vec{k}, \omega) \right]. \quad (30)$$

Several comments are in order. First, the electron-spin exchange J_0 appears in three places in Eq. (29), namely (i) in the overall shift by $-J_0 S$ of the energy argument of the \bar{G}_0^{-1} term (first term in the denominator); (ii) as an overall factor for the “self-energy” (second term in the denominator) and (iii) as a shift by $+J_0 S$ in the energy argument of the \bar{G}_0 functions appearing in the definitions of \bar{g}_{11} , etc. in the self-energy. The first and third of these are due to the zz exchange, which simply shifts the energy of the electron by $\pm J_0 S$ depending on whether its spin is parallel or antiparallel to the FM background. The second is due to the xy exchange, which facilitates the spin-flip of the electron. Therefore, the generalization to an anisotropic interaction is straightforward, for instance if $J_{0,\perp} = \lambda J_{0,z}$ then the self-energy is multiplied by λ . The exchange J between spins appears only in the magnon dispersion $\Omega_{\vec{q}}$, which enters only the \bar{g}_{11} , etc. functions appearing in the self-energy. This is not sur-

prising, since that self-energy term is due to contributions from one-magnon plus spin-up electron states. If the FM exchange between spins is longer range, one simply has to replace the magnon dispersion by the appropriate one.

Eq. (29) thus reveals that the free spin-down electron state of bare energy $\epsilon_{\vec{k}} - J_0 S$ is mixed, through spin-flipping due to the xy term, with the continuum of one-magnon plus spin-up electron states of bare energies $\epsilon_{\vec{k}-\vec{q}} + J_0 S + \Omega_{\vec{q}}$. It follows that if we are interested in having an infinitely long-lived quasiparticle state at low energies, then the electron-spin exchange must be antiferromagnetic $J_0 > 0$ (this is easily confirmed numerically). We will focus on this situation in the following (the $J_0 < 0$ case is less interesting as the low-energy dynamics is incoherent, with finite lifetime excitations).

Let us now briefly comment on other generalizations. The reason we have equations for 2×2 matrices is that, in this problem, the electron unit cell has a two-site basis.

For a basis with n different sites per unit cell one would have similar equations but for $n \times n$ matrices, where all the electron hopping information would be encoded in the corresponding \bar{G}_0 matrix. The dimensionality of the problem enters only in the sums over the Brillouin zone, i.e. in the number of integrals to be performed. Slightly more complicated is the generalization of the electron-spin exchange to longer range. This leads to the appearance of more auxiliary functions like \bar{f} and \tilde{f} , i.e. one needs to solve a linear system with more unknowns in order to find the self-energy. The various auxiliary functions correspond to the different possible phase-shifts (analogs of the $\cos(q_{x,y}a/2)$, $\sin(q_{x,y}a/2)$ appearing in the \bar{g}, \tilde{g} matrices). For example, assume that for the same system discussed here, the electron can visit all sites, including the spin sublattice. Also, assume that there is on-site exchange between the electron and the local spin, if the electron is on the spin sublattice, besides the exchange discussed here. In that case, one has to deal with 3×3 matrices (three-site basis) and there are three auxiliary functions, two similar to the ones that appeared here, and one corresponding to zero phase-shift for the on-site interaction (because of the zero phase-shift, there is no auxiliary function proportional to $\sin(0)$).

We have checked explicitly that one can also include more complicated terms, for example electron hopping accompanied by a spin-flip coupled to a spin lowering of a nearby lattice spin, like $c_{ij,1,\uparrow}^\dagger c_{ij,2,\downarrow} S_{ij}^-$ etc. (such terms have important consequences, as we discuss below). In fact, we believe that essentially any problem from this class is solvable analytically, along these general lines.

IV. RESULTS

As already mentioned, we present results for the more interesting case of an AFM electron-spin exchange, $J_0 > 0$, whose low-energy state is an infinitely-lived spin-polaron. Also, the results are for $t_1 = t_2 = t$ (s -orbitals), and t will be used as the energy unit. As discussed previously, for the simple nearest-neighbor hopping used here, the only difference for p -orbitals would be to shift the values of all momenta by $\frac{\pi}{a}(1, 1)$. For holes, t changes sign with consequences discussed where appropriate.

We begin by analyzing the dependence of the ground-state energy E_{GS} and quasiparticle weight on various parameters of the problems. In panel (a) of Fig. 2, the full lines illustrate the dependence of E_{GS} on the electron-spin exchange J_0/t , as well as the spin value S , for a fixed spin-spin exchange $J/t = 0.05$. As expected, the GS energy is lowered as both J_0 and S increase, mainly due to the favorable zz -exchange between the lattice of FM spins and the spin-down electron.

The dashed lines in Fig. 2(a) show the asymptotic expressions obtained by first order perturbation in the hopping t , in the strong-coupling limit $J_0/t \rightarrow \infty$. The agreement is very reasonable even for rather small J_0/t values, therefore it is useful to analyze this solution in some detail, to understand the nature of the spin-polaron.

In the absence of hopping, $t = 0$, we can form two sets of translationally-invariant states of well-defined momentum \vec{k} , which are ground-states of the electron-spin exchange \mathcal{H}_{exc} , namely:

$$|\vec{k}, 1\rangle = \sum_{i,j} \frac{e^{i\vec{k} \cdot \vec{R}_{ij,1}}}{\sqrt{N}} \sqrt{\frac{1}{4S+1}} \left[\sqrt{4S} c_{ij,1,\downarrow}^\dagger - \frac{1}{\sqrt{4S}} c_{ij,1,\uparrow}^\dagger (S_{ij}^- + S_{i+1,j}^-) \right] |\text{FM}\rangle \quad (31)$$

$$|\vec{k}, 2\rangle = \sum_{i,j} \frac{e^{i\vec{k} \cdot \vec{R}_{ij,2}}}{\sqrt{N}} \sqrt{\frac{1}{4S+1}} \left[\sqrt{4S} c_{ij,2,\downarrow}^\dagger - \frac{1}{\sqrt{4S}} c_{ij,2,\uparrow}^\dagger (S_{ij}^- + S_{i,j+1}^-) \right] |\text{FM}\rangle \quad (32)$$

For all of these states ($\lambda = 1, 2$),

$$\mathcal{H}_{exc} |\vec{k}, \lambda\rangle = -J_0 \left(S + \frac{1}{2} \right) |\vec{k}, \lambda\rangle.$$

The hopping \hat{T} lifts this degeneracy. In fact, it is straightforward to show that $\langle \vec{k}, \lambda | \hat{T} | \vec{k}', \lambda \rangle = 0$ while $\langle \vec{k}, 1 | \hat{T} | \vec{k}', 2 \rangle = \delta_{\vec{k}, \vec{k}'} \frac{4S+1/2}{4S+1} \epsilon_{\vec{k}}$. Thus, within this level of perturbation theory, the eigenstates are

$$|\vec{k}, \pm\rangle = \frac{1}{\sqrt{2}} \left(|\vec{k}, 1\rangle \pm |\vec{k}, 2\rangle \right) \quad (33)$$

and their corresponding energy is found to be:

$$E_{\vec{k}, \pm}^{(p)} = \pm \epsilon_{\vec{k}} \cdot \frac{4S + \frac{1}{2}}{4S + 1} + \frac{3JS}{4S + 1} - J_0 \left(S + \frac{1}{2} \right). \quad (34)$$

The middle term is due to the spin-spin FM exchange energy lost because part of the wavefunction has one spin in the background lowered by 1.

It follows that the perturbational prediction for the ground-state energy, shown in Fig. 2, is:

$$E_{GS}^{(p)} = -4t \frac{4S + \frac{1}{2}}{4S + 1} + \frac{3JS}{4S + 1} - J_0 \left(S + \frac{1}{2} \right) \quad (35)$$

In the limit of large J_0/t the agreement with the exact solution is very good. In the limit $J_0 \rightarrow 0$, and ig-

noring the small correction proportional to J (which is reasonable, given the small J/t value used), we see that $E_{GS}^{(p)} \rightarrow -4t \frac{4S+\frac{1}{2}}{4S+1} > -4t$, whereas the true GS energy cannot go above $-4t$ (this is the free-electron GS energy). For large S the difference between these two values becomes negligible, however for $S = \frac{1}{2}$ the difference is sizable, explaining the significant difference between the two curves in the low- J_0 part of Fig. 2(a).

In Fig. 2(b) we show the exact GS energies for different values of J/t and $S = \frac{1}{2}$. In the limit $J_0/t \rightarrow 0$ there is no interaction between the electron and the FM background, therefore the value of J is irrelevant. As expected from the discussion above, at large J_0/t values the GS energy increases linearly with increasing J . However, this is a small contribution for reasonably small values of J . In the following we fix $J = 0.05t$.

In Fig. 2(c) we plot the quasiparticle (qp) weights in the ground-state, defined as:

$$Z_{\lambda\lambda} = |\langle \text{FM} | c_{\vec{k}=0,\lambda,\downarrow} | \text{GS} \rangle|^2. \quad (36)$$

Clearly, these quantities give the probability to find the electron with spin-down on the sublattice $\lambda = 1, 2$, in the GS. As expected by symmetry, $Z_{11} = Z_{22}$ therefore only one is shown in Fig. 2(c), as a function of J_0/t . One immediate observation is that the qp weights saturate to finite values in the strong coupling limit $J_0/t \rightarrow \infty$, instead of becoming exponentially small, as is the case for typical polarons (where the electron binds phonons in its vicinity, due to electron-phonon coupling).¹⁸ The reason, of course, is that here the electron can bind a maximum of one magnon as opposed to an arbitrarily large number of phonons, as is the case with polarons for increasing electron-phonon coupling.

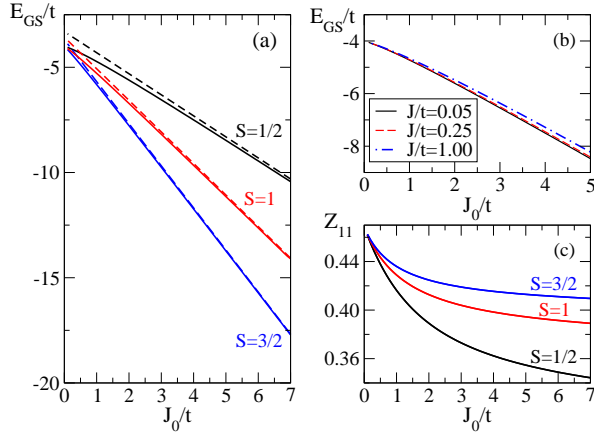


FIG. 2: (color online) (a) Spin-polaron ground-state energy, in units of t , as a function of J_0/t , for $S = \frac{1}{2}, 1$ and $\frac{3}{2}$, and $J/t = 0.05$. The full lines show the exact results, while the dashed lines give the strong-coupling perturbational limit discussed in the text; (b) Spin-polaron ground-state energy, in units of t , as a function of J_0/t , for $S = \frac{1}{2}$ and $J/t = 0.05, 0.25$ and 1.00 ; (c) Spectral weight $Z_{11} = |\langle \text{FM} | c_{\vec{k}=0,\lambda,\downarrow} | \text{GS} \rangle|^2$ as a function of J_0/t for three values of S and $J/t = 0.05$.

By direct comparison of Eqs. (31)-(33) and (1), (4), it is clear that in the strong coupling limit, the spin-down part of the low energy $|\vec{k}, +\rangle$ spin-polaron state is equal to $\sqrt{4S/(4S+1)} c_{\vec{k},+, \downarrow}^\dagger | \text{FM} \rangle$. In other words, for any momentum \vec{k} of the spin-polaron, the probability to find the electron with spin-down and the FM background undisturbed is $4S/(4S+1)$. By symmetry, it follows that $Z_{11} = Z_{22} = 2S/(4S+1)$ for all spin-polaron momenta, including the GS. This is in reasonable agreement with the values shown in Fig. 2(c), given that even $J_0/t = 7$ is not that large, therefore corrections beyond first order perturbation are not expected to be negligible.

The spin-flipped contribution to the $|\vec{k}, +\rangle$ low-energy spin-polaron state also reveals very interesting physics. Focusing on the case $S = 1/2$, we can rewrite the spin-polaron eigenstates in the strong coupling limit as:

$$|\vec{k}, +\rangle = \frac{1}{\sqrt{12N}} \sum_{ij} e^{i\vec{k} \cdot \vec{R}_{ij}} \left[\chi_{ij,\downarrow}^\dagger(\vec{k}) - S_{ij}^- \chi_{ij,\uparrow}^\dagger(\vec{k}) \right] | \text{FM} \rangle. \quad (37)$$

The operator in the bracket is recognized as creating a singlet between the spin located at site ij and the electron occupying a state centered at site ij . This singlet propagates with momentum \vec{k} through the FM background. The electron state that forms the singlet with the spin is found to be $\chi_{ij,\sigma}^\dagger(\vec{k}) = e^{i\frac{k_x a}{2}} c_{ij,1,\sigma}^\dagger + e^{i\frac{k_y a}{2}} c_{ij,2,\sigma}^\dagger + e^{-i\frac{k_x a}{2}} c_{i-1,j,1,\sigma}^\dagger + e^{-i\frac{k_y a}{2}} c_{i,j-1,2,\sigma}^\dagger$, *i.e.* a superposition of the four electronic sites surrounding the spin located at ij (site labeling is shown in Fig. 1). For larger S the solution is analogous, except one cannot speak of a “singlet” between a spin- $\frac{1}{2}$ and a spin $S > \frac{1}{2}$. However, it can be shown that the entangled electron-spin state corresponds to a total spin $S - 1/2$ (not surprising, since this is total spin that minimizes the AFM exchange energy).

In the ground-state, the coefficients are determined by the orbitals participating in the hopping. For our model we find for $\vec{k} = 0$ that $\chi_{ij,\sigma}^\dagger = c_{ij,1,\sigma}^\dagger + c_{ij,2,\sigma}^\dagger + c_{i-1,j,1,\sigma}^\dagger + c_{i,j-1,2,\sigma}^\dagger$, while for p -orbitals a similar calculation (or see $\vec{k} = \frac{\pi}{a}(1, 1)$ case) leads to $\chi_{ij,\sigma}^\dagger = -c_{ij,1,\sigma}^\dagger - c_{ij,2,\sigma}^\dagger + c_{i-1,j,1,\sigma}^\dagger + c_{i,j-1,2,\sigma}^\dagger$. In other words, the signs mirror the sign of the lobe pointing towards the central spin site.

If the charge carrier was a hole instead of an electron, because $t \rightarrow -t$ the low-energy spin-polaron eigenstate is $|\vec{k}, -\rangle$ (since now $\epsilon_{\vec{k}} > 0$). The eigenenergy is the same, but the orbital involved in the singlet is $\chi_{ij,\sigma}^\dagger(\vec{k}) = e^{i\frac{k_x a}{2}} c_{ij,1,\sigma}^\dagger - e^{i\frac{k_y a}{2}} c_{ij,2,\sigma}^\dagger + e^{-i\frac{k_x a}{2}} c_{i-1,j,1,\sigma}^\dagger - e^{-i\frac{k_y a}{2}} c_{i,j-1,2,\sigma}^\dagger$. As a result, for s -orbitals the GS orbital becomes $\chi_{ij,\sigma}^\dagger = c_{ij,1,\sigma}^\dagger - c_{ij,2,\sigma}^\dagger + c_{i-1,j,1,\sigma}^\dagger - c_{i,j-1,2,\sigma}^\dagger$, *i.e.* it has d -like symmetry. For p -orbitals it has p -like symmetry again, but is orthogonal to the one listed above for the electron.

In conclusion, the particular linear combination selected for forming the GS singlet (more generally, $S - \frac{1}{2}$ state) with the central spin is determined both by the particular orbitals involved, and by the nature – hole or

electron – of the charge carrier.

This solution is clearly analogous to the Zhang-Rice (ZR) singlet⁶ but with some differences. For one, the singlet defining the spin-polaron is here propagating in a FM, not AFM background. Second, while the ZR singlet involves a d -wave like linear combination of electronic orbitals, here the combination depends on the details of the model considered, as just discussed.

The bigger difference, of course, is that here we have spins at the Mn-like sites. Of course, spins arise from having some atomic orbital partially filled, and one can talk about a well defined spin when the number of electrons (holes) in this shell cannot change. As noted above, we can easily generalize our model to allow the extra electron (hole) to hop onto the Mn-like sites, adding a Hubbard- U penalty and/or Hundt's exchange as well, if desired. What we cannot do, at least so far, is solve exactly the more general model where electrons (holes) that are currently locked onto the Mn-like sites and constitute their spins, are allowed to hop to the other sublattice, so that a spin less than S is left behind. The difficulty is simple to see: even if one adds a charge-gap Δ , *i.e.* an energy penalty to move electrons (holes) from the Mn-like sites to the O-like sites, in any eigenstate there will be some finite probability to find any number of O-like sites occupied and the wavefunctions become too complicated. To be more precise, one can still find easily the equivalent of the FM-background state in this case, *i.e.* the ground-state in the Hilbert sector of z -axis spin NS . The case of spin $NS + n\frac{1}{2}$, when any number n of electrons (holes) with spin parallel to the background have been added in, is also trivially solved (because Hubbard on-site repulsion does not act between parallel spins, therefore both cases are essentially without interactions). However the problem corresponding to $NS - 1/2$, *i.e.* for adding a spin-down electron (hole) to the FM “background”, in other words the equivalent of the simpler problem investigated here, has proved too complicated for us so far.

However, even the asymptotic limit of our simplified model still provides a very important insight, namely that the phases of the electronic orbitals locked in the singlet with the central spin *vary inside the Brillouin zone*. In the ZR model⁶ these phases are assumed to be locked to their GS, d -wave symmetry values irrespective of the momentum of the ZR singlet. As is well known, that leads to problems with normalization of the resulting states in some regions of the BZ. What our simpler but exact solution reveals is that this is not correct: the phases of the orbitals involved in the singlet vary at different \vec{k} -points. This insight might help improve the description of the ZR singlet away from the $\vec{k} = 0$ region.

In terms of \vec{k} -dependent properties, of course we can extract not only the GS state, but the entire dispersion of the spin-polaron, by focusing on the lowest (discrete) eigenstate of momentum \vec{k} . In standard polaron physics, the polaron bandwidth is expected to become smaller (corresponding to larger effective polaron mass) as the electron-phonon coupling increases and more phonons are

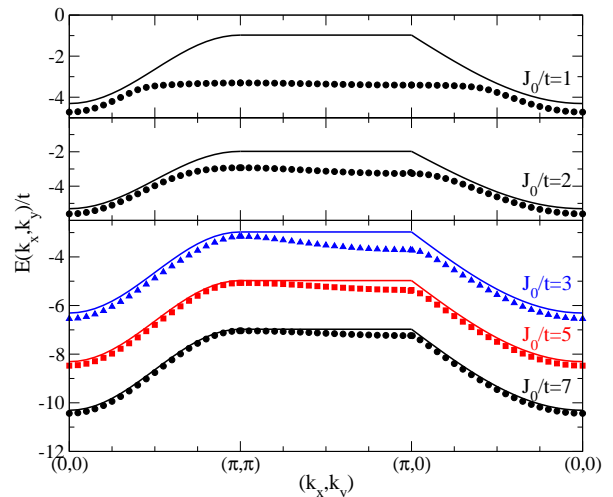


FIG. 3: (color online) Spin-polaron dispersion along lines of high symmetry in the Brillouin zone. The results (symbols) correspond to $S = \frac{1}{2}$ and $J/t = 0.05$ and, from top to bottom, $J_0/t = 1, 2, 3, 5$ and 7 . The top two cases have been plotted separately to avoid overlaps. The lines show the strong-coupling prediction $E_{\vec{k},+}^{(p)}$ of Eq. (34).

tied into the polaron cloud.¹⁸ Here we do not expect to have this problem since a maximum of one magnon can be bound to the electron, as already discussed. In fact, Eq. (34) reveals that the spin-polaron mass becomes, in the strong-coupling asymptotic limit:

$$\frac{m^*}{m} = \frac{4S + 1}{4S + \frac{1}{2}} \quad (38)$$

where m is the bare electron mass. This is interesting as it is determined only by the value S of the spins in the FM background, and independent of the coupling. The largest increase of $6/5 = 1.2$ is for spins $S = 1/2$, showing that the spin-polaron remains very light. This is not surprising, given its propagation in an FM background.

In Fig. 3 we plot the spin-polaron dispersion (lowest eigenstate of momentum \vec{k}) along lines of high symmetry inside the BZ. The full lines show the strong-coupling prediction $E_{\vec{k},+}^{(p)}$ of Eq. (34) – again, we assume s -orbitals and an electron as the charge carrier. The agreement is very good for larger J_0/t values, suggesting that the paradigm of the spin polaron as a mobile singlet of the electron in a special state and the spin at its center, must be a good description even for moderate values of J_0/t . Even for $J_0/t = 1$ the agreement is quite reasonable near the center of the BZ, but not at high \vec{k} values. This discrepancy can be understood easily as well. As discussed, the spin-polaron states come from hybridizing the non-interacting spin-down electron states of energy $\epsilon_{\vec{k}} - J_0S$ with the spin-up electron + one magnon continuum of energies $\epsilon_{\vec{k}-\vec{q}} + J_0S + \Omega_{\vec{q}}$. The hybridization will push the discrete state to lower energies, giving rise to the spin-polaron band, however it cannot change the loca-

tion of the continuum. If we ignore the $\Omega_{\vec{q}}$ term, given the small J/t , then we find that this continuum must start at $-4t + J_0S$ (inclusion of $\Omega_{\vec{q}}$ adds a small, \vec{k} -dependent correction to this value of the continuum band-edge, see results below). The spin-polaron discrete state cannot overlap with the continuum, therefore when J_0 is small, one expects the polaron dispersion to flatten out just below the continuum band-edge, which is precisely what we see for $J_0/t = 1$. As J_0/t increases the continuum moves to higher energies while the spin-polaron band moves to lower energies and becomes fully visible.

The flattening-out of the polaron dispersion just under the continuum is typical polaron physics at weak coupling.¹⁸ Of course, for conventional polarons the continuum starts at Ω above the polaron ground-state, where Ω is the energy of the Einstein phonons. This limits the polaron bandwidth, at weak coupling, to be precisely Ω . For the spin-polaron studied here, the bandwidth has little to do with the magnon energy (the FM magnons are, in fact, gapless). Instead, the relevant energy scale comes from the zz component of the exchange energy between the electron and the FM background, J_0S .

Another typical expectation for polaron physics at weak couplings is that of very small spectral weight in the BZ regions where the polaron dispersion lies just below the continuum. This is because here the largest contribution to the polaron comes from continuum states where the electron is spin-up. Consequently, the probability to find a spin-down electron, measured by the qp weights, becomes very small. This is indeed confirmed in Figs. 4, where we show the spectral weight

$$A_{\lambda\lambda}(\vec{k}, \omega) = -\frac{1}{\pi} \text{Im} G_{\lambda\lambda}(\vec{k}, \omega) \quad (39)$$

along the $k_x = k_y$ cut in the BZ. Again, by symmetry we expect $A_{11} = A_{22}$. The top panel shows the spectral weight on a linear scale. The low- k part of the spin-polaron band is clearly visible, however the region where it flattens just under the continuum has very little weight, and is not visible on this scale. In order to make low-weight features near the continuum more visible, instead of $A_{11}(\vec{k}, \omega)$, in the bottom panel we plot $\tanh[A_{11}(\vec{k}, \omega)/0.3]$. As a result, all regions with weight $A_{11} > 0.7$ are mapped into black, whereas weights below this follow a fairly linear scale down to white. This explains why the spin-polaron peak seems so wide now, although in reality it is a Lorentzian of width $\eta \rightarrow 0$. The dashed line shows the continuum band-edge, $\min_{\vec{q}}[\epsilon_{\vec{k}-\vec{q}} + J_0S + \Omega_{\vec{q}}]$. As expected, the spin-polaron dispersion flattens out just underneath it. Because its weight decreases so fast as \vec{k} increases, it is impossible to see it even on this scale for larger \vec{k} . The continuum above is also more clearly seen for smaller values of \vec{k} , with most weight around $\epsilon_{\vec{k}} - J_0S$ where the free spin-down electron would have its bare energy. The little weight that seems to “seep” below the dashed line at low- \vec{k} is due to the finite η used, we have checked that

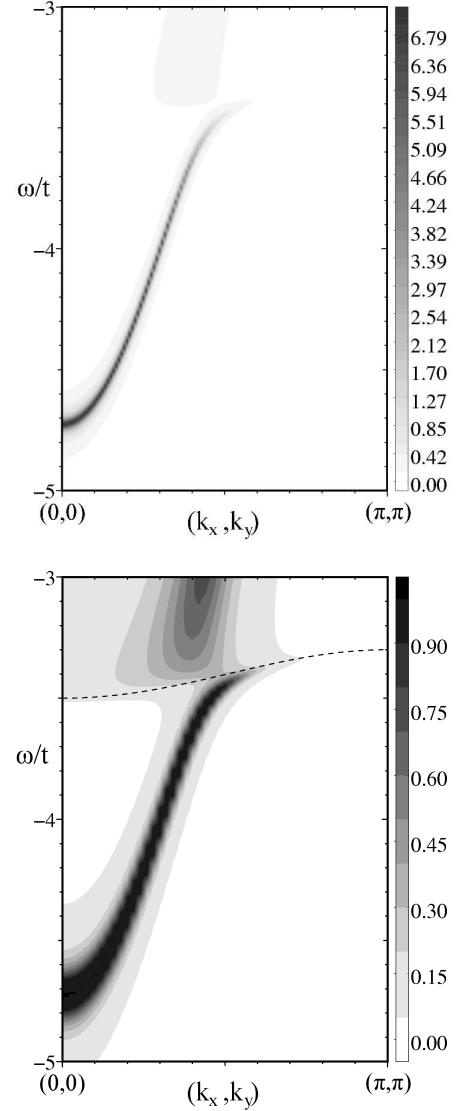


FIG. 4: Top panel: Contour plot of $A_{11}(kx, ky, \omega)$ along the $k_x = k_y$ cut in the Brillouin zone. Only the spin-polaron state is visible on this scale. Bottom panel: same as above, but plotted as $\tanh[A_{11}(kx, ky, \omega)/0.3]$ so as to make low-weight features visible. The dashed line shows the expected location of the lower edge of the continuum. Parameters are $J_0 = t = 1$, $J = 0.05$, $S = 0.5$ and $\eta = 0.02$.

indeed the continuum appears at the expected value.

As J_0 increases and the spin-polaron band moves well below the continuum, we expect to see large qp weight for the spin-polaron at all \vec{k} since the strong-coupling limit predicts a \vec{k} -independent qp weight. This is indeed the case, as shown in Fig. 5 for $J_0/t = 5$. Note that the spectral weight is now shown on a linear scale. The low-energy polaron band has the same dispersion as shown in Fig. 3, and indeed it has a fairly constant qp weight. One initial surprise is to see another coherent, infinite lifetime state just above it (and in fact degenerate with it along

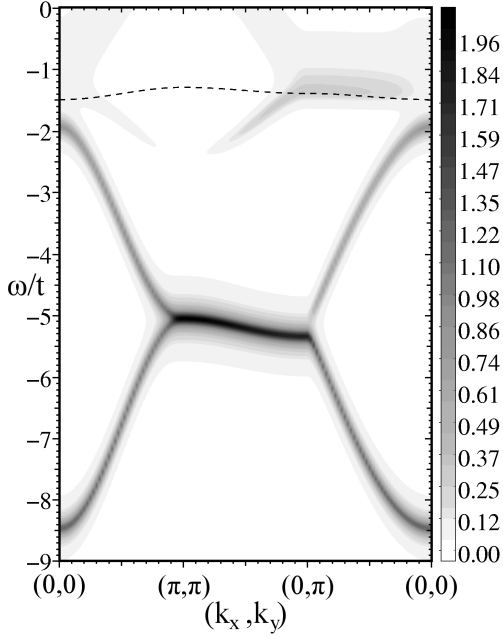


FIG. 5: Contour plot of $A_{11}(k_x, k_y, \omega)$ along several cuts in the Brillouin zone. The dashed line shows the expected location of the lower edge of the continuum. Parameters are $t = 1, J_0 = 5, J = 0.05, S = 0.5$ and $\eta = 0.1$.

the $(\pi, \pi) - (\pi, 0)$ cut, leading to a doubled qp weight there), however this is to be expected. The spin-polaron also lives on a lattice with a two-site basis, so one expects to see two bands for it, if both happen to fit below the continuum, as is the case here and for larger J_0 values. This is also in agreement with the strong-coupling limit which also predicts the two bands, see Eq. (34). From there, we see that this higher energy spin-polaron state can also be thought of as a propagating singlet, where the singlet again involves the electron in a particular wavefunction and the spin at its center. The wavefunction involves the four sites surrounding the spin, but with different \vec{k} -dependent phases (or symmetry) than for the low-energy branch.

Besides these two spin-polaron bands, Fig. 5 reveals another dispersing feature at much higher energies, of order $-2t$. That this is also a discrete (infinitely lived) state is demonstrated in Fig. 6(a), where we verify its scaling with η : doubling η halves the height of the peak and doubles its width. Thus, this is a Lorentzian of width η , and becomes a delta function as $\eta \rightarrow 0$. Note that the continuum is independent of η and begins at the expected value, indicated by the vertical line (the inset focuses on this feature and demonstrates this agreement more clearly). The continuum has very low weight, explaining why it is mostly invisible on the scale of Fig. 5.

Interestingly, we only see this higher-energy discrete state in some regions of the BZ – for example it is absent along the $(0, 0) - (0, \pi)$ line (to be more precise, we have searched with an η as low as 10^{-4} and did not see any

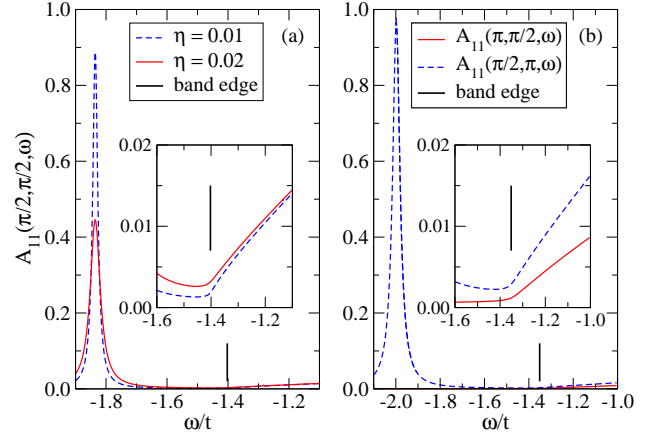


FIG. 6: (color online) (a) Spectral weight $A_{11}(\frac{\pi}{2}, \frac{\pi}{2}, \omega)$ as a function of energy, for $\eta = 0.01$ (dashed line) and $\eta = 0.02$ (full line). (b) $A_{11}(\pi, \frac{\pi}{2}, \omega)$ (full line) and $A_{11}(\frac{\pi}{2}, \pi, \omega)$ (dashed line) vs. ω , for $\eta = 0.02$. In both cases the vertical lines show the expected location of the lower band-edge of the continuum. The insets show the same quantities, but with the focus on the lower band-edge of the continuum. The parameters are $t = 1, J_0 = 5, J = 0.05$ and $S = \frac{1}{2}$.

features just below the gap. Of course, this does not rule out a state with an extremely low qp weight). The apparent “disappearance” near (π, π) is due to vanishing qp weight, but the state exists in that region. Another interesting feature is demonstrated by Fig. 6(b), which shows $A_{11}(\vec{k}, \omega)$ at two points that one would normally consider equivalent, namely $(\pi, \frac{\pi}{2})$ and $(\frac{\pi}{2}, \pi)$. While the former shows a big qp peak just above $-2t$, the latter shows no weight at this energy. The explanation is that by symmetry one needs to have $A_{11}(k_x, k_y, \omega) = A_{22}(k_y, k_x, \omega)$, since “1” and “2” refer to states on the x , respectively y -rungs. However, for $k_x \neq k_y$, there is no requirement that $A_{11}(k_x, k_y, \omega) = A_{11}(k_y, k_x, \omega)$ and indeed we see that this is not the case. Fig. 6(b) thus suggests that the disappearance of this qp state along some directions is due to symmetries, which result in orthogonality between the spin-down free electron state and the true eigenstate. Polarization-dependent spectroscopies should be able to detect these variations between A_{11} and A_{22} .

Regarding the origin of this high-energy qp state, this seems to be standard polaron physics. Holstein polarons at strong couplings are also known to have a so-called “second bound state”.¹⁸ It is essentially an internal excited state of the polaron, possible if the interaction and so the binding energy with its cloud is strong enough.

These two examples, together, are enough to give us intuition about the evolution of the spectral weight in such models as J_0 increases. For small values only the lowest spin-polaron band is visible in regions where it is well below the continuum. In the regions where the continuum forces it to flatten, the qp is extremely small. As J_0 increases, more and more of the low-energy spin-polaron band emerges below the continuum. Then the

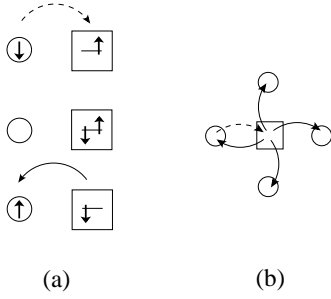


FIG. 7: (a) Illustration of exchange between the charge carrier and the impurity spin (depicted as a box), arising from virtual hopping of the charge carrier to the spin site, and back. (b) The same type of process can result in charge carrier hopping with spin flip, if the charge carrier moves to another site.

upper spin-polaron band starts to emerge as well and the part that is below the continuum is clearly visible, the rest is flattened and with low qp weight. This is the case *e.g.* for $J_0 = 3$ (not shown) where the entire lower band and about one third of the upper band are visible below the continuum. For even larger J_0 both spin-polaron bands are visible, and at yet higher values, more bound states can split-off from the continuum. The number of qp bands and their weights is therefore very sensitive to strength of the coupling.

Before concluding, we must make one more important comment. In the model considered here we assumed that the charge carrier interacts with the spins only through exchange. This exchange comes from virtual hopping of the charge carrier to the spin site and back. Fig. 7(a) illustrates one such possible scenario, leading to AFM exchange if a single half-filled orbital gives rise to the impurity spin. However, the charge carrier could hop off to any of the nearest neighbor sites of the impurity spin, since it does not necessarily have to return to the original site. Such processes are illustrated in Fig. 7(b) and result in effective charge carrier hopping with possible spin-flip correlated with a spin flip of the impurity spin. The energy scale for such processes is the same as for the AFM exchange, however their sign can be either negative or positive, depending on whether the hopping integrals along the relevant links have the same, or opposite signs. This, of course, depends on the orbitals involved both at the charge carrier and the spin site.

Such hopping + spin-flip processes can be treated exactly in our approach, as already stated. They can have dramatic effects, as we illustrate now with a simple example. Consider the spin S at site (ij) and its four neighboring charge sites, which we label anticlockwise as $1 = (ij, 1)$, $2 = (ij, 2)$, $3 = (i-1, j, 1)$ and $4 = (i, j-1, 2)$. Four symmetric linear combinations can be built from these, namely $\chi_{s\sigma} = \frac{1}{2}(c_{1\sigma} + c_{2\sigma} + c_{3\sigma} + c_{4\sigma})$; $\chi_{d\sigma} = \frac{1}{2}(c_{1\sigma} - c_{2\sigma} + c_{3\sigma} - c_{4\sigma})$; $\chi_{p1\sigma} = \frac{1}{2}(c_{1\sigma} + c_{2\sigma} - c_{3\sigma} - c_{4\sigma})$ and $\chi_{p2\sigma} = \frac{1}{2}(c_{1\sigma} - c_{2\sigma} - c_{3\sigma} + c_{4\sigma})$. Consider the impurity spin lowering part of the Hamiltonian we have worked with so far, $J_0 S^- (c_{1\uparrow}^\dagger c_{1\downarrow} + c_{2\uparrow}^\dagger c_{2\downarrow} + c_{3\uparrow}^\dagger c_{3\downarrow} + c_{4\uparrow}^\dagger c_{4\downarrow}) =$

$J_0 S^- (\chi_{s\uparrow}^\dagger \chi_{s\downarrow} + \chi_{d\uparrow}^\dagger \chi_{d\downarrow} + \chi_{p1\uparrow}^\dagger \chi_{p1\downarrow} + \chi_{p2\uparrow}^\dagger \chi_{p2\downarrow})$ *i.e.* all these symmetrized orbitals interact equally strongly with the impurity, and could participate in the “singlet”. Which happens to be the GS is chosen by the signs of the hoppings and charge carrier, as discussed. If hopping + spin flip processes are included, the results are very different. Assume for example that all hopping integrals between the 4 sites and the impurity site have the same sign. In this case, $J_0 S^- c_{1\uparrow}^\dagger c_{1\downarrow} \rightarrow J_0 S^- (c_{1\uparrow}^\dagger + c_{2\uparrow}^\dagger + c_{3\uparrow}^\dagger + c_{4\uparrow}^\dagger) c_{1\downarrow}$, since as illustrated in Fig. 7(b), the charge carrier removed from site 1 can emerge at any of the spin’s neighbor sites. The same is true for all other terms, and adding them together, we obtain a total equal to $4J_0 S^- \chi_{s\uparrow}^\dagger \chi_{s\downarrow}$. In other words, in this case only the s -symmetry orbital can participate in the singlet (which state is selected depends, obviously, on the relative signs for the hopping between charge sites and the impurity site). As a result, we expect to see a single spin-polaron state at $\vec{k} = 0$, corresponding to a “singlet” involving this allowed orbital, and the other spin-polaron states discussed for the simple model will vanish from the spectrum.

V. SUMMARY AND CONCLUSIONS

To summarize, we claim that essentially any problem that involves a charge carrier interacting with a fully polarized FM background can be solved exactly, irrespective of the complexity of the sublattices involved or the range of the exchanges or other complications. Of course, calculations become more complex as one makes the model more complicated, but the exact solution following the approach suggested here should always be possible.

We exemplified it on a relatively simple, yet interesting two-dimensional case which we believe illustrates most of the physics that can be expected in such systems. It allows us to elucidate the nature of the spin-polaron quasiparticle, which at strong coupling is a singlet (more generally, the maximally polarized state with spin $S - \frac{1}{2}$) similar to the Zhang-Rice solution. However, we show that the orbitals participating to the electronic wavefunction that locks into the singlet with the lattice spin, have phases that vary as a function of the singlet’s momentum. In the ground state they have the signs consistent with the symmetry of the orbitals involved and also determined by the type of charge carrier. Moreover, since on complex lattices one can form multiple such linear combinations which can participate in the singlet, it is possible to see more than one spin-polaron band below the continuum. If however hopping + spin-flip terms are included, some of these spin-polaron bands will be removed because of symmetry considerations.

We hope that these insights may help solve some of the known issues regarding the normalization of the ZR singlet, which is an essential ingredient in the cuprate physics. Extensions of the solution to AFM backgrounds are very desirable, although clearly much more complicated. We plan to investigate such problems next.

As far as uses of doped FM insulators for spintronics applications are concerned, this work suggests that materials with an AFM exchange J_0 between the charge carriers and the local spins could be very interesting. For instance, consider a pulse of unpolarized charge carriers created in such a medium, for instance by optical means. If they are placed in an electric field, the charge carriers with spin parallel to the FM background will propagate with a different speed than the charge carriers with spin antiparallel to the FM background, since the latter are dressed by magnons and become heavier spin-polarons while the former propagate as bare particles. Both types propagate coherently (at least at $T = 0$) so this suggests that in time a pulse of unpolarized carriers will separate spatially into two spin-polarized pulses traveling at different speeds. Ingenious use of such difference between the two spin polarizations may open the way towards using

such materials as sources or detectors of spin-polarized currents, which are essential components for spintronic devices. Of course, issues such as the effect of finite- T and finite charge carrier concentrations need to be understood first, however this seems to be a promising line of investigation.

Acknowledgments

This work was supported by NSERC and the CIFAR Nanoelectronics (M.B.) and Quantum Materials (G.S.) programs. Part of this work was carried out at the Kavli Institute for Theoretical Physics, which is supported by NSF under Grant No. PHY05-51164.

-
- ¹ J. B. Torrance, M. W. Shafer, and T. R. McGuire, Phys. Rev. Lett. **29**, 1168 (1972).
 - ² P. Schiffer, A. P. Ramirez, W. Bao, and S-W. Cheong, Phys. Rev. Lett. **75**, 3336 (1995).
 - ³ J. G. Bednorz and K. A. Muller, Z. Phys. B **64**, 189 (1986).
 - ⁴ P. W. Anderson, Science **235**, 1196 (1987).
 - ⁵ A. S. Mishchenko, N. V. Prokof'ev, and B. V. Svistunov, Phys. Rev. B **64**, 033101 (2001).
 - ⁶ F. C. Zhang and T. M. Rice, Phys. Rev. B **37**, 3759 (1988).
 - ⁷ E. L. Nagaev, Zh. Eksp. Teor. Fiz **56**, 1013 (1969) [Sov. Phys. JETP **29**, 545 (1969)].
 - ⁸ Yu. A. Izyumov and M. V. Medvedev, Zh. Eksp. Teor. Fiz **59**, 553 (1970) [Sov. Phys. JETP **32**, 302 (1971)].
 - ⁹ S. Methfessel and D. C. Mattis, in Handbuch der Physik, edited by S. Flügge (Springer-Verlag, Berlin, 1968), Vol. XVIII/1, pp. 419-424.
 - ¹⁰ P. Richmond, J. Phys. C **3**, 2402 (1970).
 - ¹¹ B. S. Shastry and D. C. Mattis, Phys. Rev. B **24**, 5340 (1981).
 - ¹² W. Nolting, Phys. Status Solidi B **96**, 11 (1979)
 - ¹³ S. G. Ovchinnikov and L. Ye. Yakimov, Phys. Sol. State **45**, 1479 (2003).
 - ¹⁴ see, for instance, W. Nolting, G. G. Reddy, A. Ramakanth, and D. Meyer, Phys. Rev. B **64**, 155109 (2001) and R. Schiller and W. Nolting, Phys. Rev. B **60**, 462 (1999).
 - ¹⁵ R. Vollmer, M. Etzkorn, P. S. Anil Kumar, H. Ibach, and J. Kirschner, Phys. Rev. Lett. **91**, 147201 (2003).
 - ¹⁶ T. Saitoh, A. Sekiyama, K. Kobayashi, T. Mizokawa, and A. Fujimori, D. D. Sarma, Y. Takeda, M. Takano Phys. Rev. B **56**, 8836 (1997).
 - ¹⁷ G. D. Mahan, Many-Particle Physics (Plenum, New York, 1981).
 - ¹⁸ extensive results for the Holstein polaron are shown in M. Berciu and G. L. Goodvin, Phys. Rev. B **76**, 165109 (2007); G. L. Goodvin, M. Berciu, and G. A. Sawatzky, Phys. Rev. B **74**, 245104 (2006) and references therein.